

Gravitational Lensing of CMB by Quasars in SDSS-IV

Jiashu Han ¹★, Simone Ferraro^{2,3}, Elena Giusarma^{4,5} and Shirley Ho ^{2,3,4}

¹*Department of Physics, University of California, Berkeley, CA 94720, U.S.A.*

²*Lawrence Berkeley National Laboratory, 1 Cyclotron Rd, Berkeley, CA 94720, U.S.A.*

³*Berkeley Center for Cosmological Physics, University of California Berkeley, Berkeley, CA 94720, U.S.A.*

⁴*Center for Computational Astrophysics, Flatiron Institute, 162 5th Avenue, New York, NY 10010, U.S.A.*

⁵*McWilliams Center for Cosmology, Department of Physics, Carnegie Mellon University, Pittsburgh, PA 15213, USA*

13 September 2018

ABSTRACT

In this paper we study the cross-correlation between the *Planck* CMB lensing convergence map and the eBOSS quasar overdensity obtained from the Sloan Digital Sky Survey (SDSS) IV, in the redshift range $0.9 < z < 2.2$. We detect a CMB lensing convergence-quasar angular cross power spectrum with 5.4σ significance. The cross power spectrum provides a measurement of the quasar clustering bias with little to no systematics. The redshift distribution of the quasar sample has a median redshift $z \approx 1.55$, and an effective redshift about 1.51. The best fit bias of the quasar sample is $b_q = 2.43 \pm 0.45$, corresponding to halo mass of $\log_{10} \left(\frac{M}{h^{-1}M_{\odot}} \right) = 12.54^{+0.25}_{-0.36}$. This is broadly consistent with the previous literature on quasars within the similar redshift range and selection. However, being obtained in cross-correlation with CMB lensing, we expect it to be robust to a wide range of possible systematic effects that may contaminate the auto correlation of quasars. We check for various systematic effects from both CMB lensing and Quasar overdensity maps, and found that all systematics to be consistent with null within 2σ . The data is not sensitive to a possible scale dependence of the bias at present, but we expect that as the number surveyed quasars increases (in future surveys such as DESI), it is likely that strong constraints on the scale dependence of the bias can be obtained.

Key words: large-scale structure of Universe – quasars: general – cosmic background radiation

1 INTRODUCTION

The cosmic microwave background (CMB) temperature fluctuations provide invaluable information about our Universe, and can give extremely tight constraints on cosmological parameters (Kofman et al. 1993; Hinshaw et al. 2012; Planck Collaboration et al. 2015b, 2018). The primary CMB anisotropy encodes information about the primordial universe, measured at $z \approx 1100$, the redshift of last scattering. However, since the discovery of the CMB, a lot of progress has also been made on the secondary CMB anisotropies, such as gravitational lensing, the thermal and kinetic Sunyaev-Zel’dovich (tSZ, kSZ) effects (Sunyaev & Zel’dovich 1980), and the integrated Sachs-Wolfe effect (ISW) (Sachs & Wolfe 1967). These effects can act as foreground for the primary CMB, but they also encode information about the growth of structure at lower redshifts, a powerful probe of Dark Energy, Modified Gravity and neutrino masses (Hirata et al.

2008; Lewis & Challinor 2006). In addition to CMB temperature and polarization fluctuations, independent cosmological probes include: Cepheids (Spergel et al. 1997), supernovae (Baron et al. 2004; Bridle et al. 2001) to large scale surveys of galaxies (SDSS-IV, Blanton et al. (2017)), Lyman- α forests (Weinberg et al. 2003) and galaxies covering a large range of luminosities, masses and redshifts (Abazajian et al. 2016).

The primary CMB dominates over the secondary anisotropies at the large angular scales. However, because the secondary anisotropies are tracers of various types of large scale structures (LSS) (Aghanim et al. 2008), they can be easily detected through cross-correlation with the LSS. In particular, CMB lensing can trace the matter density field at intermediate redshifts (Zaldarriaga & Seljak 1999; Hirata et al. 2008). As the CMB photons travel to the observer, they can be gravitationally deflected by the matter distribution in the universe. The deflections leave imprints on the observed CMB temperature fluctuations and distort the original temperature map. We can extract information about the matter distribution of the universe at these red-

★ E-mail: jiashu.han@berkeley.edu

shifts by studying the distortions of the CMB due to lensing (Lewis & Challinor 2006).

Weak lensing of the CMB introduces correlations in the Fourier modes of the temperature and polarization maps, and therefore the CMB lensing deflection field \mathbf{d} can be estimated by measuring the correlations between Fourier modes of the observed temperature/polarization fluctuations that are uncorrelated in the unlensed fluctuations (Hu & Okamoto 2002). The related CMB lensing convergence map used in this work was published by the Planck Collaboration (Planck Collaboration et al. 2015c).

Besides CMB lensing, we are also interested in the growth of the LSS, and quasars are good tracers of the LSS at intermediate redshifts. Quasars are luminous accreting supermassive black holes at the centers of distant galaxies (Salpeter 1964). Like galaxies, they are tracers of the 3D distribution of dark matter at different redshifts. With the understanding that almost every galaxy hosts a supermassive black hole at its center (Kormendy & Richstone 1995), quasars can be thought as a phase in the galaxy evolution. Properties of quasars, such as the characteristic mass of the their host halos (Tinker et al. 2010), can be inferred by studying the relationship between the dark matter distribution and quasar clustering. The information about quasar properties can reveal much about the growth of structure over the history of the universe (Marziani & Sulentic 2014; Mortlock 2015).

Both CMB lensing and the observed quasar overdensity depend on the projected matter overdensity, so the CMB lensing convergence and the quasar overdensity should have a relatively strong correlation (Peiris & Spergel 2000). Due to clustering, quasars are biased tracers of the underlying matter density field (Kaiser 1984), meaning that the observed cross power spectrum and the theoretical cross power spectrum are related by some factor (Peacock & Smith 2000; Seljak 2000). This factor, called the quasar bias, parametrizes the properties of the clustering of quasars and encapsulates the information about the processes of galaxy formation and evolution that are currently not very well understood (Amendola et al. 2017). Measuring this bias factor would be crucial to the understanding of galaxy formation and the evolution of supermassive black holes within the standard structural formation framework (Shen et al. 2009).

Laurent et al. (2017), have analyzed the auto-correlation of the eBOSS quasars, and put constraints on the quasar bias, as well as the corresponding host halo mass. In this paper, we use an alternative way to constrain the quasar bias, by cross-correlating the CMB lensing data from Planck and quasars drawn from eBOSS Data Release 14 (Dawson et al. 2016). We measure a quasar bias that is consistent with the auto-correlation result. We then calculate the corresponding characteristic host halo mass of the quasars. All calculations assume a cosmology with Planck 2015 parameters (Planck Collaboration et al. 2015b). This paper is organized into the following parts: in Section 2 we present the theoretical background of quasar linear bias and the CMB lensing-quasar angular cross power spectrum. Section 3 includes the data samples and estimators we used to estimate the observed power spectrum. In Section 4, we present estimates of the cross power spectrum, the quasar bias, and the characteristic host halo mass. In Section 5, we check for er-

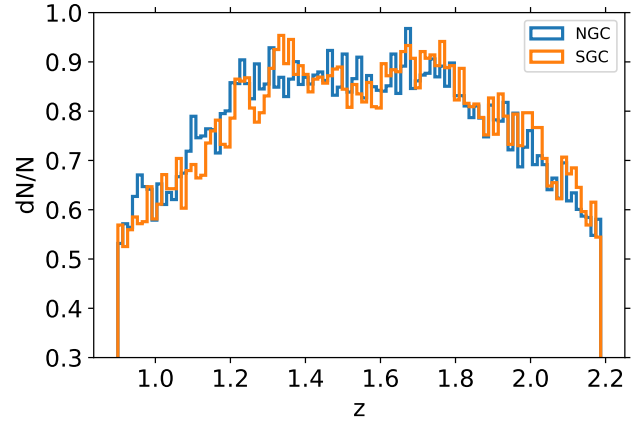


Figure 1. The redshift distribution of the selected quasars in the range $0.9 < z < 2.2$.

rors, systematic effects and perform a null test. We conclude in Section 6.

2 THEORETICAL BACKGROUND

2.1 Overview

Quasars reside in the nuclei of distant galaxies and are hosted by dark matter halos as the result of clustering, so the number density of quasars is related to the dark matter density by a bias factor, i.e. $\delta_q = b_q \delta_m$ (White & Rees 1978). The amplitude of the deflection by CMB lensing in a certain direction depends on the projected dark matter density in that direction, as described by the lensing convergence in Equation 1, so we would expect the quasar number density to be correlated with CMB lensing convergence (Peiris & Spergel 2000). The quasar bias parametrizes the properties and processes of quasar clustering that we currently do not fully understand. Current galaxy models do not provide adequate information to predict the bias, but the bias parameter can be obtained from observational data (Contreras et al. 2013; Amendola et al. 2017). An accurate model of the quasar bias could marginalize over the systematics introduced by the bias and allow the testing of the validity of various galaxy formation and evolution models.

2.2 Angular cross power spectrum

In order to relate CMB lensing to matter density, we can describe the effect of CMB lensing using the lensing convergence, defined as $\kappa \equiv -\frac{1}{2} \nabla \cdot \mathbf{d}$, where \mathbf{d} is the lensing deflection field. The lensing convergence is a weighted projection of the matter overdensity in some direction \hat{n} along the line of sight (Lewis & Challinor 2006):

$$\kappa(\hat{n}) = \int_0^{z_{CMB}} \frac{cdz}{H(z)} W(z) \delta_m(\chi(z)\hat{n}, z) \quad (1)$$

where $z_{CMB} \approx 1100$ is the redshift at the last scattering surface, $H(z)$ is the Hubble parameter at redshift z , $W(z)$ is the CMB lensing kernel, $\delta_m(\chi(z)\hat{n}, z)$ is the matter overdensity

at redshift z in the direction \hat{n} , and $\chi(z)$ is the comoving distance at redshift z . Assuming a flat universe, $W(z)$ is given by

$$W(z) = \frac{3H_0^2\Omega_{m,0}}{2c^2}\chi(z)\left(1 - \frac{\chi(z)}{\chi_{CMB}}\right) \quad (2)$$

where χ_{CMB} is the comoving distance to the last scattering surface, H_0 is the current Hubble parameter, and $\Omega_{m,0}$ is the current matter density parameter. Since the lensing potential ϕ is a 2D projection of the gravitational potential, we can assume CMB lensing as an unbiased tracer of the underlying matter overdensity field (Lewis & Challinor 2006).

The quasar overdensity field can be described by a window function $f(z)$ (Peiris & Spergel 2000) such that the projected surface density is $q(\hat{n}) = \int_0^{z_{CMB}} dz f(z)\delta_m(\chi(z)\hat{n}, z)$:

$$f(z) = \frac{b(z)dN/dz}{\int dz' \frac{dN}{dz'}} + \frac{3}{2H(z)}\Omega_0 H_0^2(1+z)g(z)(5s-2) \quad (3)$$

where the first term is the normalized, bias-weighted redshift distribution of the quasars. The second term is the magnification bias, which accounts for the change in the density of the sources due to lensing magnification (Moessner et al. 1997; Scranton et al. 2005). For our sample, this term is negligible compared to the redshift distribution and we ignore it for simplicity.

On large scales, we expect the bias is to be independent of scale. On smaller scales, however, the scale-dependence of the bias has been supported by many observations and analyses on two-point statistics, galaxy counts, and gravitational lensing (Amendola et al. 2017; Giusarma et al. 2018).

Many bias models have been proposed. We will consider an effective power law parametrization of the scale dependence of the bias:

$$b(k) = b_1 + b_2 \left(\frac{k}{k_0}\right)^n \quad (4)$$

where k_0 is an arbitrary reference scale that we set to be $1h \text{ Mpc}^{-1}$. The case $n = 0$ corresponds to a scale-independent bias.

Desjacques et al. (2016) and Modi et al. (2017) reported an $n = 2$ behavior at intermediate scales for the linear halo bias, based on results from N-body simulations. We will test this form for the scale-dependent quasar bias.

If the selection functions of the dark matter tracers are slowly varying compared to the scale we are probing, the Limber approximation (Limber 1954; Lewis & Challinor 2006) is expected to be valid at $\ell \gtrsim 30$. Assuming a flat universe, the quasar-CMB lensing convergence angular cross-power spectrum is given by:

$$C_l^{kq} = \int \frac{dz}{\chi^2(z)}(1+z)W(z)f(z)P_{mm}\left(k = \frac{l}{\chi(z)}, z\right) \quad (5)$$

where $f(z)$ is the bias-weighted redshift distribution, and $P_{mm}(k, z)$ is the 3D matter power spectrum.

An advantage of using the cross-correlation between CMB lensing and quasars over doing quasar auto-correlation, is that the quasar clustering-matter cross power spectrum has a linear dependence on the quasar bias, from the bias-weighted redshift distribution. Moreover, measuring this cross-correlation in addition to the auto-correlation of quasars helps break the degeneracy between quasar bias

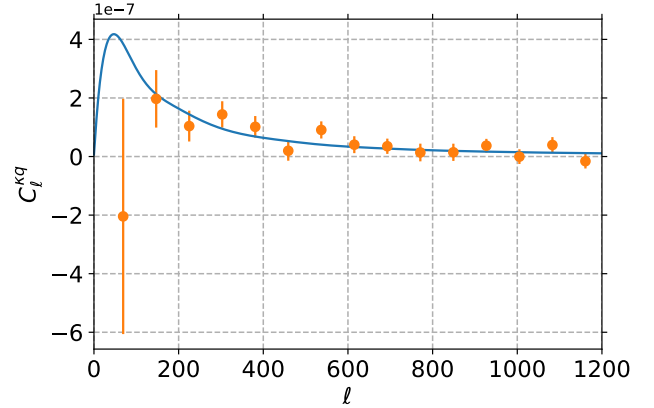


Figure 2. The CMB lensing-quasar overdensity angular cross-power spectrum. The data points are in orange, and the blue solid curve is the calculated theory curve. The significance of the cross-power spectrum signal is 5.4σ .

b_q and amplitude of fluctuations¹ σ_8 . The cross-correlation is also less likely to be affected by systematics in the quasar sample.

3 DATA AND METHODS

3.1 CMB lensing map

We use the CMB lensing convergence map published by the Planck Collaboration (Planck Collaboration et al. 2015c). The *Planck* satellite, which was launched on May 14, 2009, observed the temperature and polarization fields of the cosmic background radiation over the whole sky at various frequencies from August 12, 2009 to October 23, 2013. Maps of the temperature and polarization fields of the CMB covering 70% of the sky are produced (Planck Collaboration et al. 2015a). The Planck minimum-variance CMB lensing potential field is reconstructed using the CMB maps produced by the SMICA code, and combines the five quadratic estimators of the correlations of the CMB temperature (T) and polarizations (E, B). The CMB lensing map provides an estimate of the lensing potential power spectrum at the multipole range $40 < \ell < 400$, and is checked for systematic effects due to the Galaxy, dust emission, point sources, and instrumental noise. These systematic effects are found to be small compared to the statistical errors (Planck Collaboration et al. 2015c). The map is in HEALPix format with $N_{\text{side}} = 2048$.

3.2 Quasar map

We use quasars from the extended-Baryon Oscillation Spectroscopic Survey (eBOSS, Dawson et al. (2016), Zhao 2016), which started in July 2014, as an extension to the Baryon Oscillation Spectroscopic Survey (BOSS) (Dawson et al. 2013). BOSS probed the BAO at a scale of roughly $100 h^{-1}$

¹ This is because the auto-correlation measures $b_q^2\sigma_8^2$, while the cross correlation is proportional to $b_q\sigma_8^2$

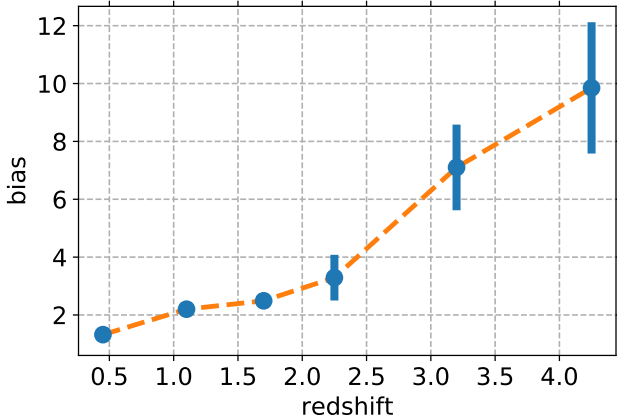


Figure 3. The fiducial bias-redshift model used in the calculation, obtained by interpolating the data points in Shen et al. (2009). The paper also provides estimates of the error in the quasar bias, which are shown as error bars in the plot. The dashed line in orange is the interpolated result.

Mpc, using mostly galaxies at $z < 0.7$ and neutral hydrogen clouds in the Lyman- α forest at $z > 2.1$.

eBOSS aims to probe four different dark matter tracers at redshift ranges that are not covered in previous surveys, and map the large scale structures over the redshift range $0.6 < z < 2.2$, which is previously unconstrained by BOSS. The full eBOSS quasar catalog (Myers et al. 2015) is expected to contain 500,000 spectroscopically-confirmed quasars over an area of 7500 deg² by the end of the survey and provide the first BAO distance measurement over the range $0.9 < z < 2.2$. The eBOSS quasars will also provide tests of General Relativity on the cosmological scales through measurements of the redshift-space distortion, and new constraints on the summed mass of all known neutrino species.

We use the eBOSS Data Release 14 quasar catalog (Pâris et al. 2018), which contains 142,017 quasars between $0.9 < z < 2.2$, and divide the sample into 100 redshift bins. The redshift distribution of the selected quasars is shown in Fig. 1. We construct an overdensity map ($q_i = \frac{n_i - \bar{n}}{\bar{n}}$, where i is the pixel number) of these quasars. The map is converted into HEALPix format with $N_{\text{side}} = 2048$ to match the resolution of the CMB lensing convergence map.

3.3 Estimator for the angular power spectrum

We use a pseudo- C_l estimator (Lewis et al. 2011) to calculate the angular cross-power spectrum from the data

$$\hat{C}_l^{\kappa q} = \frac{1}{f_{\text{sky}}^{\kappa q} (2l+1)} \sum_{m=-l}^l \kappa_{lm}^* q_{lm} \quad (6)$$

where $f_{\text{sky}}^{\kappa q}$ is the fraction of the sky shared by the quasar map and the CMB lensing convergence map. κ_{lm} is the spherical harmonic transform of the CMB lensing convergence map, and q_{lm} is the spherical harmonic transform of the quasar overdensity map.

In the Fisher approximation, the theoretical error in each bin A of $\hat{C}_l^{\kappa q}$ can be estimated using (Cabr e et al.

2008)

$$\frac{1}{\sigma^2(A)} = \sum_{l_{\min}(A) < l < l_{\max}(A)} \frac{f_{\text{sky}}(2l+1)}{(C_l^{\kappa q})^2 + C_l^{\kappa \kappa} C_l^{q q}} \quad (7)$$

where $C_l^{\kappa \kappa}$ and $C_l^{q q}$ are the CMB lensing and quasar auto-power spectra, including both signal and noise. The contribution of error from the $C_l^{\kappa \kappa} C_l^{q q}$ term should dominate the contribution from the cross term. The auto-spectra can be estimated similarly:

$$\hat{C}_l^{\kappa \kappa} = \frac{1}{f_{\text{sky}}^{\kappa} (2l+1)} \sum_{m=-l}^l |\kappa_{lm}|^2 \quad (8)$$

and

$$\hat{C}_l^{q q} = \frac{1}{f_{\text{sky}}^q (2l+1)} \sum_{m=-l}^l |q_{lm}|^2 \quad (9)$$

where f_{sky}^{κ} is the sky fraction of the CMB lensing convergence map, and f_{sky}^q is the sky fraction of the quasar overdensity map. We bin the cross-power spectrum into 15 bands in the range $30 < \ell < 1200$. We choose $\ell_{\min} = 30$ because the Limber approximation breaks down on larger scales, and $\ell_{\max} = 1200$ because of uncertainty on modeling the bias and powers spectrum on smaller scales.

4 RESULTS

4.1 Cross-correlation

The cross-correlation results are shown in Fig. 2. The theoretical curves are calculated using Equation 5. We use the redshift distribution in Fig. 1 and the CMB lensing kernel in Equation 2. The theory curve should not be sensitive to binning and interpolation, since the weighting functions are slowly varying with redshift. We use CAMB (Lewis et al. 2000) to compute the matter power spectrum. The nonlinear matter power spectrum (HALOFIT, Smith et al. 2003; Takahashi et al. 2012) is used in this calculation. The linear matter power spectrum produces similar results because the signal mainly comes from angular scales ($\ell < 600$) corresponding to the linear part of the matter power spectrum (Sherwin et al. 2012).

We assume a fiducial bias-redshift model from Shen et al. (2009) in the theory calculation, shown in Fig. 3. The theory curve is a good fit to the data. With 14 degrees of freedom, the chi-squared value for the best-fit theory curve is $\chi_{\text{th}}^2 = 12.9$. The significance of the cross-correlation is $\sqrt{\chi_0^2 - \chi_{\text{th}}^2} = 5.4\sigma$, where χ_0^2 is the chi-squared value for the null hypothesis.

Despite the theory curve being a good fit to the data points, the first bin deviates significantly (more than 1σ) from the theoretical prediction and shows an anti-correlation between the CMB lensing map and the quasar overdensity, albeit having a large uncertainty. Pullen et al. (2016) also reported a deficit of power in the low ℓ region of the CMB lensing-galaxy angular cross power spectrum. We do not have an explanation for the cause of this deficit of power.

| n | b_0 | $\sigma(b_0)$ | b_1 | $\sigma(b_1)$ | χ^2 |
|-----|-------|---------------|---------|---------------|----------|
| -2 | 2.80 | 0.50 | -0.0010 | 0.0006 | 11.0 |
| -1 | 3.53 | 0.81 | -0.067 | 0.041 | 11.2 |
| 0 | 2.43 | 0.45 | - | - | 12.9 |
| 1 | 1.85 | 0.89 | 6.37 | 8.71 | 13.3 |
| 2 | 2.26 | 0.59 | 13.0 | 33.3 | 13.7 |

Table 1. Selected results for the scale-dependent bias fit. In the third row, $n = 0$ corresponds to a scale-independent bias.

4.2 Quasar bias

The fiducial bias-redshift model used in the calculation is obtained by interpolating the data in Shen et al. (2009). The model was constructed by calculating the amplitude of the quasar correlation function from the SDSS DR5 quasar sample. Although it uses a different quasar catalog than the one in our analysis, we choose this as a convenient model because the theoretical cross-power spectrum does not have a strong dependence on the form of the bias model. The fiducial model is shown in Fig. 3. From this model we find $b_q/b_{\text{fid}} = 1.01 \pm 0.19$. At the effective redshift of our quasar sample ($z \approx 1.51$), the fiducial model gives a bias $b_{\text{fid}} = 2.4$. Combining these results we get a quasar linear bias of $b_q = 2.43 \pm 0.45$.

We also fit for the scale-dependent bias in Equation 4, by fixing n at various values. Table 1 shows some of the results. In the $n = 2$ case, we have $b_1 = 2.26 \pm 0.59$ and $b_2 = 13.0 \pm 33.3$, with 5.4σ significance. We conclude that the data does not yield a good constraint on the scale dependent bias.

4.3 Quasar host halo mass

As shown in Fig. 3, the quasar bias generally increases with redshift, and the bias is expected to increase with halo mass. However, at higher redshifts, the halos also have less time to grow. Therefore, we would expect a roughly constant halo mass-redshift relation.

We use the bias model provided in Tinker et al. (2010) to relate the scale-independent quasar bias to the peak height of the linear density field, $\nu = \frac{\delta_c}{\sigma(M)}$, where $\delta_c = 1.686$ is the critical overdensity for collapse, and calculate a corresponding characteristic host halo mass. We assume the ratio between the halo mass density and the average matter density of universe is $\Delta = 200$. We find the characteristic host halo mass to be $\log_{10} \left(\frac{M}{h^{-1} M_\odot} \right) = 12.54^{+0.25}_{-0.36}$. This is consistent with previous estimates (White et al. 2012; Laurent et al. 2017) at similar redshifts.

5 MEASUREMENT SYSTEMATICS AND UNCERTAINTIES

5.1 Systematic effects

Residual foregrounds in the CMB map that are correlated with the large scale structure probed by the eBOSS quasars can lead to biases to CMB lensing cross-correlation (van Engelen et al. 2014; Osborne et al. 2014; Ferraro & Hill 2018). Mitigation strategies have been proposed (Madhavacheril & Hill 2018; Schaan & Ferraro 2018), and based on previous

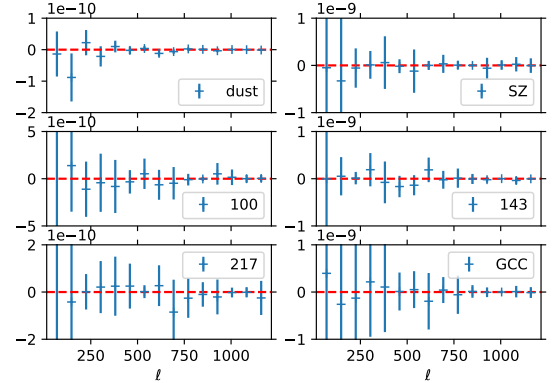


Figure 4. Check for possible systematic effects on the cross power spectrum due to contaminants. Here we show the right hand side of Eq. 10 for different foregrounds. The dust plot is the bias due to dust emission. The SZ plot is the bias due to the Planck SZ catalogue. The 100, 143, and 217 plots are the biases from Planck Catalogue of Compact Objects, corresponding to the labeled frequency. The GCC plot is the bias from the Planck Galactic cold clumps.

work we expect the bias to cross-correlations with Planck lensing to be at most a few percent, considerably smaller than our statistical significance.

Nonetheless, we check for contamination from galactic dust emission, point sources, and SZ effect. We use the Second Planck SZ Catalogue (Planck Collaboration et al. 2015e), which includes sources detected through the SZ effect (Sunyaev & Zel'dovich 1980), the Schlegel et al. (1998) dust infrared emission map for estimation of CMB radiation foregrounds, the Planck Catalogue of Galactic cold clumps (Planck Collaboration et al. 2015f), and the overdensity maps constructed from the Second Planck Catalogue of Compact Sources (Planck Collaboration et al. 2015d) at frequencies 100 GHz, 143 GHz, and 217 GHz.

If we systematic effects added linearly to the observed CMB lensing map and quasar map (Ross et al. 2011; Ho et al. 2012), the bias to the cross correlation would be given by (Giannantonio et al. 2016):

$$\Delta \hat{C}_l^{\kappa q} = \sum_s \frac{\hat{C}_l^{\kappa s} \hat{C}_l^{q s}}{\hat{C}_l^{s s}} \quad (10)$$

where s is the map for the systematics. While the lensing map is obtained through non-linear operations on the CMB map, and therefore the assumption of linearity is not satisfied, estimating the quantity above is still a powerful null-test. If significant contamination was found, Eq. 10 should not be used to correct for the bias, but more sophisticated mitigation techniques should be employed (Schaan & Ferraro 2018; Madhavacheril & Hill 2018; Osborne et al. 2014).

Fig. 4 shows the right hand side of Eq. 10. The effects are consistent with null at most scales and we conclude that there is no significant systematic effects due to the contaminants considered above. We calculate the overall systematic error by adding the average absolute biases at each angular scale, weighted by the inverse variance, and find it to be less than 7% of the signal.

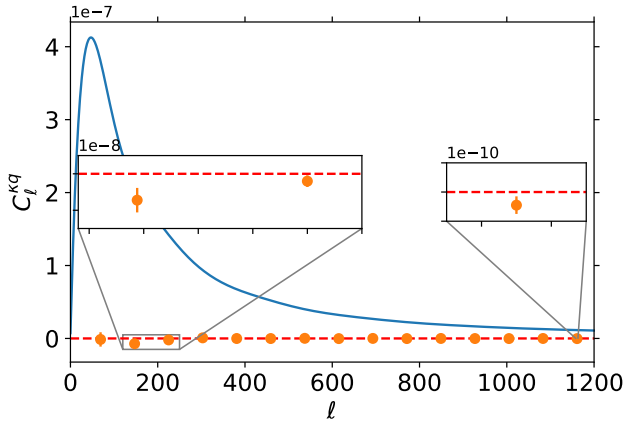


Figure 5. The cross-power spectrum from the null test. The blue curve is the best-fit theoretical cross-power spectra. The result is consistent with zero correlation.

5.2 Null test

We use a simple null test (Sherwin et al. 2012) on the CMB lensing-quasar overdensity cross power spectrum to check our result and procedure by cross-correlating the CMB lensing convergence map on one part of the sky with the quasar map on another part of the sky. The result of the null test is shown in Fig. 5. Most bins are consistent with the null result, with a significance of 0.05σ , and the best fit chi-square value for the null hypothesis is 11.23, with 14 degrees of freedom.

5.3 Covariance matrix

The theoretical error bar for each bin is calculated using Equation 7, which assumes the bins are independent. Limited sky fraction may induce correlation between ℓ bins, and this assumption is only valid when the bins are relatively large ($\Delta\ell \gtrsim 2/f_{\text{sky}}$) (Gaztañaga et al. 2012; Cabré et al. 2008). In our case, the bins are large and should be roughly independent in the limit of large $\Delta\ell$.

To compute the full covariance matrix of \hat{C}_l^{kq} , we use quasar mocks and CMB lensing simulations. The quasar mocks are taken from the QSO EZmocks (effective Zel’dovich approximation mock catalogues) (Chuang et al. 2014), which include 1000 realizations of the quasar map with the same number of randomly distributed sources. The CMB lensing simulations include 100 realizations of simulated lensing convergence maps (Planck Collaboration et al. 2015c) containing both signal and noise. We cross correlate 100 pairs of the quasar mocks and lensing simulations, and calculate the average of the cross power spectra, to estimate the covariance matrix $\text{cov}[i, j] = \langle (C(i) - E(C(i)))(C(j) - E(C(j))) \rangle$.

The off-diagonal elements of the covariance matrix are small compared to the diagonal elements (Fig. 6), and the diagonal elements mostly agree with the theoretical values, calculated using Equation 7. In both the theoretically predicted error and the covariance matrix, the error in the cross power spectrum decreases with increasing ℓ for $\ell < 1200$. On smaller scales, the error increases again, due to a combina-

tion of shot noise of the quasars and reconstruction noise in the lensing map.

The central value and the uncertainty of the bias estimate change slightly when we use the full covariance matrix, which gives a bias of 2.42 ± 0.44 with a significance of 5.4σ and $\chi_{\text{th}}^2 = 13.9$ for 14 degrees of freedom.

6 CONCLUSIONS

We studied the cross-correlation between the Planck CMB lensing convergence map and the eBOSS DR14 quasar map at redshift range $0.9 < z < 2.2$, with an effective redshift of $z_{\text{eff}} \approx 1.51$, and measure the quasar bias. We found correlation between CMB lensing and the eBOSS quasars, and a quasar bias $b_q = 2.43 \pm 0.45$ at 5.4σ significance, using the theoretically calculated covariance matrix. This is consistent with the result in Laurent et al. (2017). We obtain the covariance matrix from the quasar mocks and lensing simulations, and it is consistent with the theoretical covariance matrix. While the theory curve is a good fit for most of the scales, the first bin shows low cross-correlation between CMB lensing and quasar clustering. The origin of this deficit of power at low- ℓ is not known at present.

Using the Tinker et al. (2010) model of the relation between halo mass function and clustering, we calculate a characteristic host halo mass for the eBOSS DR14 quasar catalog: $\log_{10} \left(\frac{M_{200}}{1h^{-1}M_{\odot}} \right) = 12.54^{+0.25}_{-0.36}$. This is consistent with previous estimates of the quasar host halo mass at similar redshifts (White et al. 2012; Laurent et al. 2017). We also attempted to fit for the scale dependent bias, using a power law model with a scale independent term and a scale dependent term, but did not find a tight constraint for the scale dependent term with any power law indices.

For the error analysis, we performed a simple null test for the cross power spectrum, and the result is mostly consistent with null, with the exception of two low- ℓ bins and one near ℓ_{max} . We checked for several systematics and found no significant contributions from the considered contaminants.

The significance and accuracy of the quasar bias measurement depend on the sample size and number density of the quasar survey (Seljak et al. 2009), so we would expect the signal-to-noise ratio of the detection using this method to improve, as eBOSS continues to expand its sample size (Dawson et al. 2016) and new surveys such as DESI (DESI Collaboration et al. 2016) and Euclid (Laureijs et al. 2011) become operational. This will provide more precise measurements of the quasar bias as a function of redshift, scale, etc, and open paths to better understanding of the various properties of quasars, including the host halo mass and duty cycle (Martini & Weinberg 2001). The improved bias measurement could also provide good constraints on the galaxy formation models (Contreras et al. 2013), general relativity and modified gravity (Acquaviva et al. 2008), and the properties of dark matter and dark energy (Das & Spergel 2009).

ACKNOWLEDGEMENTS

We thank Siyu He, Anthony Pullen, Emmanuel Schaan, Blake Sherwin, Jeremy Tinker and Michael Wilson for help-

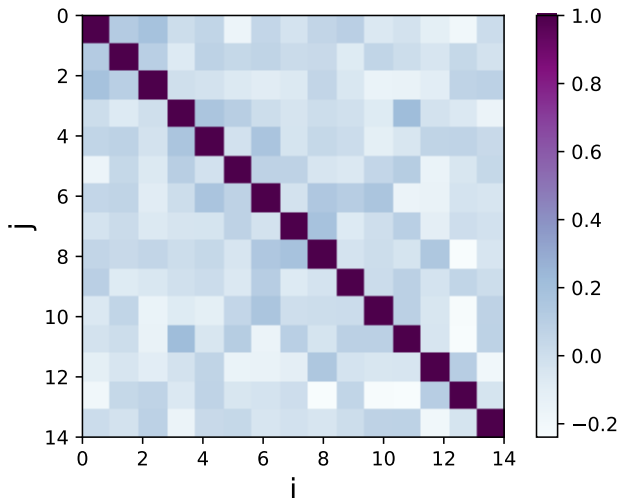


Figure 6. The normalized covariance matrix of the angular cross power spectrum ($(\text{cov}[i, j] / \sqrt{\text{cov}[i, i] * \text{cov}[j, j]})$), where i and j are labels of the bins.

ful discussions. J.H. would like to thank Stephen Ebert for helpful comments on the paper. This work is based on observations made by the Planck satellite and the Apache Point Observatory. The Planck project (<http://www.esa.int/Planck>) is funded by the member states of ESA, and NASA. The SDSS-IV project (<http://www.sdss.org/>) is funded by the participating institutions, the National Science Foundation, the United States Department of Energy, and the Alfred P. Sloan Foundation. S.F. is funded by a Miller Fellowship at the University of California, Berkeley. S.H. thanks NASA for their support in grant number: NASA grant 15-WFIRST15-0008 and NASA ROSES grant 12-EUCLID12-0004. E.G. is supported by NSF grant AST1412966 and by the Simons Foundation through the Flatiron Institute.

REFERENCES

- Abazajian K. N., et al. 2016, preprint, ([arXiv:1610.02743](https://arxiv.org/abs/1610.02743))
- Acquaviva V., Hajian A., Spergel D. N., Das S. 2008, *Phys. Rev. D*, **78**, 043514
- Aghanim N., Majumdar S., & Silk J. 2008, Reports on Progress in Physics, **71**, 066902. ([arXiv:0711.0518](https://arxiv.org/abs/0711.0518))
- Amendola L., Menegoni E., Di Porto C., Corsi M., Branchini E. 2017, *Phys. Rev. D* **95**, 023505
- Baron E., Nugent P. E., Branch D., Hauschildt P. H. 2004, *ApJ*, **616**, L91
- Blanton M. R., et al. 2017, *AJ*, **154**, 28
- Bridle S. L., Zehavi I., Dekel A., Lahav O., Hobson M. P., Lasenby A. N. 2001, *MNRAS*, **321**, 333
- Cabr e A., Fosalba P., Gazta aga E., Manera M. 2008, *MNRAS*, **381**, 11
- Contreras S., Baugh C. M., Norberg P., Padilla N. 2013, *MNRAS*, **432**, 2717
- Chuang C-H, Kitaura F-S, Prada F., Zhao C., Yepes G. 2014, *MNRAS*, **446**, 2621
- Das S., Spergel D. N. 2009, *Phys. Rev. D*, **79**, 043509
- Dawson K. S., Schlegel D. J., Ahn C. P., et al. 2013, *AJ*, **145**, 10
- Dawson K. S., Kneib J-P, Percival W. J., et al. 2016, *AJ*, **151**, 44
- DESI Collaboration et al. 2016, preprint, ([arXiv:1611.00036](https://arxiv.org/abs/1611.00036)).
- Desjacques V., Jeong D., Schmidt F., 2016, *Physics Reports*, **733**, 1. ([arXiv:1611.09787](https://arxiv.org/abs/1611.09787))
- Ferraro, S., & Hill, J. C. 2018, *Phys. Rev. D*, **97**, 023512
- Gazta aga E., et al., 2012, *MNRAS*, **422**, 2904
- Giannantonio T., et al., 2016, *MNRAS*, **456**, 3213
- Giusarma E., et al., 2018, preprint. ([arXiv:1802.08694](https://arxiv.org/abs/1802.08694))
- Hinshaw G., et al. 2012, *ApJS*, **208**, 19
- Hirata C. M., Padmanabhan N., Seljak U., Schlegel D., Brinkmann J. 2004, *Phys. Rev. D*, **70**, 103501
- Hirata C. M., Ho S., Padmanabhan N., Seljak U., Bahcall N. 2008, *Phys. Rev. D*, **78**, 043520
- Ho S., Cuesta A., et al. 2012, *ApJ*, **761**, 14
- Hu W. & Okamoto T. 2002, *ApJ*, **574**, 566
- Kaiser, N. 1984, *ApJ*, **284**, L9
- Kofman, L. A., Gnedin, N. Y., & Bahcall, N. A. 1993, *ApJ*, **413**, 1
- Kormendy J. & Richstone D. 1995, *ARA&A*, **33**, 581
- Kuntz A. 2015, *A&A*, **584**, A53
- Laureijs R., et al. 2011, preprint, ([arXiv:1110.3193](https://arxiv.org/abs/1110.3193))
- Laurent P., Eftekharzadeh S., Le Goff J.-M. et al. 2017, *JCAP*, **07**, 017
- Lewis A., Challinor A., & Lasenby, A. 2000, *ApJ*, **538**, 473
- Lewis A. & Challinor A. 2006, *Phys. Rept.*, **429**, 1. [arXiv:astro-ph/0601594](https://arxiv.org/abs/astro-ph/0601594)
- Lewis A. & Challinor A., & Hanson, D. 2011, *JCAP*, **03**, 018
- Limber D. N. 1954, *ApJ*, **119**, 655
- Madhavacheril, M. S., & Hill, J. C. 2018, [arXiv:1802.08230](https://arxiv.org/abs/1802.08230)
- Martini P. & Weinberg D. H. 2001, *ApJ*, **547**, 12
- Marziani P., Sulentic J. 2014, *Advances in Space Research*, **54**, 1331
- Modi C., Castorina E., Seljak U. 2017, *MNRAS*, **472**, 3959
- Moessner R., Jain B., Villumsen J. V. 1997, *MNRAS*, **294**, 291. ([arXiv:astro-ph/9708271](https://arxiv.org/abs/astro-ph/9708271))
- Mortlock D. J. 2015, preprint. ([arXiv:1511.01107](https://arxiv.org/abs/1511.01107))
- Myers A. D., Palanque-Delabrouille N., Prakash A., et al. 2015, *ApJS*, **221**, 27. [arXiv:1508.04472](https://arxiv.org/abs/1508.04472)
- Osborne, S. J., Hanson, D., & Dor e, O. 2014, *J. Cosmology Astropart. Phys.*, **3**, 024
- P aris I., Petitjean P., Aubourg E., et al. 2018, *A&A*, **613**, A51
- Peiris H. V. & Spergel D. N. 2000, *ApJ*, **540**, 605
- Peacock J. A. & Smith R. E. 2000, *MNRAS*, **318**, 1144
- Planck Collaboration et al. 2015a, preprint, ([arXiv:1502.01582](https://arxiv.org/abs/1502.01582))
- Planck Collaboration et al. 2015b, *A&A*, **594**, A13
- Planck Collaboration et al. 2015c, *A&A*, **594**, A15
- Planck Collaboration et al. 2015d, *A&A*, **594**, A26
- Planck Collaboration et al. 2015e, *A&A*, **594**, A27
- Planck Collaboration et al. 2015f, *A&A*, **594**, A28
- Planck Collaboration et al. 2018, preprint, ([arXiv:1807.06209](https://arxiv.org/abs/1807.06209))
- Pullen A. R., Alam S., He S., Ho S. 2016, *MNRAS*, **460**, 4098
- Ross A. J., Ho S., et al., 2011, *MNRAS*, **417**, 1350
- Sachs, R. K. & Wolfe, A. M. 1967, *ApJ*, **147**, 73
- Salpeter E. E. 1964, *ApJ*, **140**, 796
- Schaan, E., & Ferraro, S. 2018, [arXiv:1804.06403](https://arxiv.org/abs/1804.06403)
- Schlegel D. J., Finkbeiner D. P., Davis M. 1998, *ApJ*, **500**, 525
- Scranton R., et al. 2005, *ApJ*, **633**, 589
- Seljak U. 2000, *MNRAS*, **318**, 203
- Seljak U., Hamaus N., Desjacques V. 2009, *Phys. Rev. Lett.*, **103**, 091303
- Shen Y., Strauss M. A., Ross N. P., et al. 2009, *ApJ*, **697**, 1656
- Sherwin B. D., Das S., et al. 2012, *Phys. Rev. D* **86**, 083006
- Smith R. E., Peacock J. A., Jenkins A., et al. 2003, *MNRAS*, **341**, 1311
- Spergel D. N., Bolte M., Freedman W. 1997, *PNAS*, **94**, 6579
- Sunyaev R. A., & Zel'dovich Ya. B. 1980, *ARA&A*, **18**, 537
- Takahashi R., Sato M., Nishimichi T., Taruya A., Oguri M. 2012, *ApJ*, **761**, 152

- Tinker J. L., Robertson B. E., Kravtsov A. V., et al. 2010, [ApJ](#), **724**, 878
- van Engelen, A., Bhattacharya, S., Sehgal, N., et al. 2014, [ApJ](#), **786**, 13
- Weinberg D. H., Dav'e R., Katz N., Kollmeier J. A. 2003, [AIP Conference Proceedings](#) **666**, 157
- White S. D. M. & Rees M. J. 1978, [MNRAS](#), **183**, 341
- White M., Myers A. D., Ross N. P., et al. 2012, [MNRAS](#), **424**, 933
- Zaldarriaga M. & Seljak U. 1999, [Phys. Rev. D](#) **59**, 123507
- Zhao G.-B., Wang Y., Ross A. J., et al. 2016, [MNRAS](#), **457**, 2377

This paper has been typeset from a $\text{\TeX}/\text{\LaTeX}$ file prepared by the author.